Journal of Power Sources 196 (2011) 8544–8548

Contents lists available at ScienceDirect

Journal of Power Sources

journal homepage: www.elsevier.com/locate/jpowsour

Short communication

Infiltrated multiscale porous cathode for proton-conducting solid oxide fuel cells

Fei Zhao, Qiang Liu, Siwei Wang, Fanglin Chen*

Department of Mechanical Engineering, University of South Carolina, Columbia, SC 29208, USA

ARTICLE INFO

Article history:
Received 7 March 2011
Received in revised form 4 June 2011
Accepted 6 June 2011
Available online 12 June 2011

Keywords:
Solid oxide fuel cells
Infiltration
Multiscale porous
Cell polarization resistance

ABSTRACT

A $Sm_{0.5}Sr_{0.5}CoO_{3-\delta}$ (SSC)–$BaZr_{0.1}Ce_{0.7}Y_{0.2}O_{3-\delta}$ (BZCY) composite cathode with multiscale porous structure was successfully fabricated through infiltration for proton-conducting solid oxide fuel cells (SOFCs). The multiscale porous SSC catalyst was coated on the BZCY cathode backbones. Single cells with such composite cathode demonstrated peak power densities of 0.289, 0.383, and 0.491 W cm^{-2} at 600, 650, 700 °C, respectively. Cell polarization resistances were found to be as low as 0.388, 0.162, and 0.064 Ω cm^2 at 600, 650 and 700 °C, respectively. Compared with the infiltrated multiscale porous cathode, cells with screen-printed SSC–BZCY composite cathode showed much higher polarization resistance of 0.912 Ω cm^2 at 600 °C. This work has demonstrated a promising approach in fabricating high performance proton-conducting SOFCs.

1. Introduction

Solid oxide fuel cell (SOFC) has been regarded as one of the most promising devices to efficiently convert the chemical energy from the fuel to electricity with low to zero emissions [1]. However, SOFCs are currently not economically competitive to the existing power generation methods due to the problems associated mainly with high temperature operation (>800 °C). Lowering the SOFC operating temperature is expected to greatly reduce the cost for materials used for the SOFC components and significantly improve the SOFC durability. Compared with SOFCs based on oxygen ion conductors such as yttria-stabilized zirconia (YSZ), SOFCs based on proton conductors such as doped $BaCeO_3$ have attracted much attention due to their lower activation energy for proton transport and higher conductivity at low and intermediate temperatures, resulting in feasible SOFC operation in the temperature range of 600–700 °C [2–5]. However, lowering the operation temperature is always accompanied by the increase in cell resistance dominated by the ohmic resistance from the electrolyte as well as the cathode interfacial polarization resistance for Ni-based anode supported cells [6]. In the past two decades many effective approaches have been established to fabricate thin film electrolyte to reduce the electrolyte ohmic resistance [7–10]. Therefore, exploiting novel cathode materials or unique cathode microstructures to reduce the cathode polarization resistance is critical in the development of high performance proton conducting SOFCs [11].

To date, several new electrode architectures have been developed to create durable, effective, and functional electrode for intermediate temperature SOFCs [12–15]. Among them, multiscale porous mixed ionic and electronic conducting cathodes are very inspiring due to the capability of combined gas transport and extended length of triple-phase boundary (TPB) regions where oxygen reduction reaction taking place [16]. Since oxygen diffuses through the cathode pores to TPBs and gas transport depends largely on the architecture of the cathode, multiscale porous cathode can offer rapid mass transport through macropores and provide quick gas adsorption/desorption and more active sites for oxygen reduction through high surface areas in the mesopores [17]. Consequently, enhanced cathode performance is expected for the cathode with multiscale porous structure. For example, a dual-scale porous $Sm_{0.5}Sr_{0.5}CoO_{3-\delta}$ (SSC)–$Gd_{0.1}Ce_{0.9}O_{1.95}$ (GDC) cathode fabricated using a poly(methyl methacrylate) colloidal-crystal templating method was reported by Zhang et al., showing a low cathodic interfacial resistance of 0.39 Ω cm^2 at 750 °C [17], offering potentially high cell performance for intermediate temperature SOFCs.

A modified self-assembly approach has recently been developed to synthesize multiscale porous metal oxides [18,19]. Macropores can be created by using urea as a leavening agent while mesopores inside the shells or walls of the macropores are generated by the self-assembly process [20–22]. For instance, $La_{0.5}Sr_{0.5}Co_{0.5}Fe_{0.5}O_{3-\delta}$ (LSCF) cathode material synthesized using this approach showed a honeycomb-like microstructure with disordered hierarchical pores, exhibiting high specific surface area of 65 m^2 g^{-1} and large pore volume of 0.11 cm^3 g^{-1}, which are expected to be extremely favorable to oxygen reduction process in the cathode [18]. However, it turns out to be very difficult to

* Corresponding author. Tel.: +1 803 777 4875; fax: +1 803 777 0106.
E-mail address: chenfa@cec.sc.edu (F. Chen).

0378-7753/$ – see front matter © 2011 Elsevier B.V. All rights reserved.
doi:10.1016/j.jpowsour.2011.06.029

directly apply such multiscale porous material as cathode in SOFCs. The main reason is that the multiscale porous material does not possess adequate thermal and mechanical strength to maintain such distinct multiscale porous structure during the typical screen-printing cathode preparation process, which involves grinding or ball-milling cathode powder with a binder to make a cathode ink, screen-printing the cathode ink to an electrolyte surface, and then firing the cathode in a temperature range of 900–1200 °C to obtain good contact of the cathode to the electrolyte [23]. To overcome the damage of the multiscale porous cathode structure, infiltration process has been employed in this work to in situ prepare the multiscale porous cathode. Infiltration method has been frequently used to fabricate nanostructured electrodes, involving adsorption and subsequent decomposition of metal salts at relatively low temperatures [24,25]. Relatively low fabricating temperature used in the infiltration process is in favor of maintaining the catalytic activity of the cathode and its structural integrity [26]. For example, Wu et al. successfully incorporated SSC into a pre-sintered porous $BaCe_{0.8}Sm_{0.2}O_{2.9}$ (BCS) backbone to form an effective SSC–BCS composite cathode, showing a low cell polarization resistance of 0.076 Ω cm^2 at 700 °C [27]. Not only good electrochemical activity but also excellent durability was manifested by infiltrated cathodes. Composite cathode with $Sm_{0.2}Ce_{0.8}O_{1.9}$ (SDC) as electrolyte backbone and $La_{0.6}Sr_{0.4}CoO_{3-\delta}$ (LSC) as infiltrated cathode catalyst showed an interfacial resistance of 0.29 Ω cm^2 without significant performance degradation at 600 °C for 100-day operation with thermal cycling treatments [28].

In this study, we have developed a multiscale porous composite cathode of SSC–$BaZr_{0.1}Ce_{0.7}Y_{0.2}O_{3-\delta}$ (BZCY) for proton-conducting intermediate temperature SOFCs. The BZCY backbone of the composite cathode is expected to provide continuous pathway for proton conduction while the SSC cathode catalyst coated on the BZCY cathode backbone with disordered multiscale porous structure is expected to exhibit enhanced gas diffusion and enlarged electrochemical reaction sites for oxygen reduction. The SSC is fabricated in situ by infiltrating a modified self-assembly precursor, followed by calcinating at 900 °C for 2 h to form multiscale porous structure.

2. Experimental

2.1. Power fabrication

Powders of BZCY and $BaCe_{0.7}In_{0.3}O_{3-\delta}$ (BCI) were synthesized by a modified citrate–nitrate combustion process [29,30]. BZCY was used as proton-conducting phase in the electrodes due to its high proton conductivity [31], and BCI was used as the proton-conducting electrolyte film due to its high chemical stability and good sinterbility [32,33]. NiO was prepared using a glycine–nitrate combustion process [14]. SSC powder was produced by a modified self-assembly method as described previously [18]. Stoichiometric amount of $Sm(NO_3)_3{\cdot}6H_2O$, $Sr(NO_3)_2$, and $Co(NO_3)_2{\cdot}6H_2O$ was added into Pluronic P123 ($EO_{20}PO_{70}EO_{20}$, Mav = 5800) alcohol–water solution. Urea was then added as the leavening agent to form SSC precursor. Urea decomposes to gases (NH_3 and CO_2) to create macropores and P123 was used as surfactant to generate mesopores through the self-assembly process. The SSC precursor was then calcined at 900 °C for 2 h to remove organics and form final powder.

2.2. Cell fabrication

Anode substrates consisting of NiO, BZCY and graphite with a weight ratio of 3:2:1 were mixed and pressed uniaxially into pellets with a diameter of 15 mm, followed by firing at 800 °C for 2 h to form porous anode substrates. BCI electrolyte membranes were deposited on the as-prepared anode substrates with a suspension-coating method as described previously [14]. BCI powder was ball-milled with an organic dispersant and absolute ethanol for 48 h to form a stable suspension. The suspension was then drop-coated onto the anode substrates using an injector. The green electrolyte/anode bi-layers were subsequently co-sintered at 1400 °C for 5 h to form half cells with dense BCI electrolyte membranes (~18 μm). BZCY slurry was prepared by ball-milling BZCY powder, graphite, and ethyl cellulose–terpineol for 24 h and then screen-printed onto the BCI electrolyte surface of the as-prepared half cells, followed by sintering at 1300 °C for 5 h to form a pseudo-single cell consisting of a porous NiO–BZCY anode substrate (~0.4 mm), a dense BCI electrolyte membrane and a porous BZCY cathode backbone (~80 μm). SSC was incorporated into the porous BZCY backbone by infiltration method [14,18]. The SSC precursor, which was the same solution as described in the powder fabrication section, was infiltrated into the porous BZCY backbone, followed by firing at 500 °C for 10 min with a ramping and cooling rate of 1 °C min^{-1}. Infiltration was repeated until the SSC loading was about 75% of the weight of the BZCY backbone. The infiltrated product was finally fired at 900 °C for 2 h to form an infiltrated cell. For comparison, SSC–BZCY cathode ink with the same mass ratio used in the infiltrated cathode was fabricated by mechanically mixing ethyl cellulose–terpineol, SSC and BZCY powders. The ink was then applied on the as-prepared half cells, followed by firing at 900 °C for 2 h to form a screen-printed cell.

2.3. Cell characterization

Single cells were sealed on an alumina tube using silver paste. The cells were tested with humidified hydrogen (3% H_2O, 40 mL min^{-1}) as the fuel and ambient air as the oxidant. All cells were stabilized at 600 °C and NiO was fully reduced to Ni in situ before any electrochemical tests were performed. Cell power output performance and AC impedance spectra were measured using a Versa 3 electrochemical station with an applied 10 mV sinusoidal voltage in the frequency range of 1 MHz to 0.01 Hz. Phase formation and morphologies of samples were determined using a Mini X-ray powder diffractometer and a scanning electron microscope (FEI-200), respectively.

3. Results and discussion

3.1. Phase formation

Shown in Fig. 1 are the X-ray diffraction patterns of BZCY powder, SSC powder and infiltrated SSC–BZCY composite cathode. It can be clearly seen that only peaks related to perovskite phase are observed for the BZCY and SSC powders after calcination. No impurity peaks are found for the infiltrated SSC–BZCY composite cathode fired at 900 °C for 2 h, consistent with Yang's study [34].

3.2. Microstructures of the composite cathodes

The cross-sectional views of the infiltrated and screen-printed SSC–BZCY cathodes are shown in Fig. 2. Dendritic structure with high porosity are found for the BZCY cathode backbone as shown in Fig. 2(a), indicating uninterrupted paths for proton conduction and facile gas transport features favorable for the oxygen reduction process. After firing the infiltrated precursor, the dendritic BZCY cathode backbones were subsequently coated by SSC catalysts, showing a specific surface area of 1.079 m^2 g^{-1}. The SSC has three-dimensionally open pores with dimensions of hundreds to thousands of nanometers randomly distributed on the BZCY backbone as shown in Fig. 2(b). Fig. 2(c) shows a screen-printed

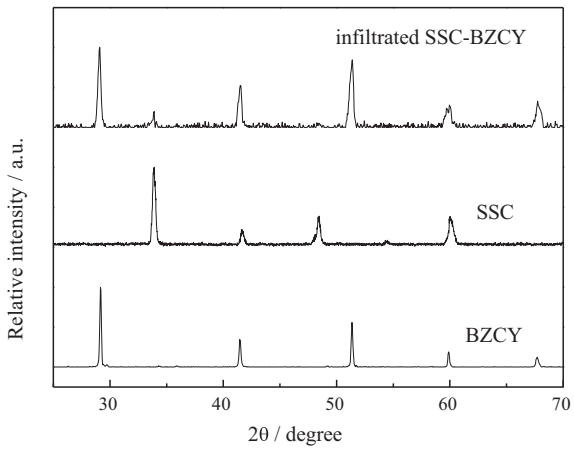

Fig. 1. X-ray diffraction patterns of BZCY powder, SSC powder and infiltrated SSC–BZCY composite cathode.

SSC–BZCY composite cathode fabricated from the slurry consisting of the SSC and BZCY powders. The SSC powder has similar multiscale microstructure as demonstrated in our previous work [18,19]. As shown in Fig. 2(c), the cathode reveals a randomly distributed mixture of SSC and BZCY with no visible the multiscale porous SSC structure, probably destroyed during the mechanically mixing process. Fig. 2(d) shows a cross-section photograph of the freshly infiltrated cathode at high magnification. Macropores produced by a leavening process of urea can be observed in Fig. 2(d), and the distribution of these pores is more disordered probably due to the inhomogenous and complicated environment compared with the SSC powder fabricated from precursor solutions in beakers [18]. Small-sized pores and nanoparticles with a size range from 50 to 100 nm generated by the self-assembly process are also found inside the shells or walls of the macropores. Such multiscale porous microstructure and nano-sized particles are expected to significantly enhance cathode performance due to improved gas diffusion and extended length of TPB sites.

3.3. Single cell performance

The performance of anode-supported proton-conducting cell was investigated using humidified H_2 (3% H_2O) as fuel with a flow fuel rate of 40 mL min^{-1} and ambient air as oxidant. Shown in Fig. 3(a) are the current–voltage curves and the corresponding power densities for cells based on infiltrated and screen-printed cathodes at different operating temperatures. The open-circuit voltages (OCVs) for the cell based on infiltrated cathode were 1.07, 1.048, and 1.022 V at 600, 650, and 700 °C, respectively. These OCV values were higher than those for cell based on similar BCI electrolyte film reported by Bi et al. [32], which were 1.015 and 0.977 V at 600 and 700 °C, respectively, indicating that the BCI electrolyte film in this work was sufficiently dense and exhibited negligible electronic conduction. Peak power densities of 0.289,

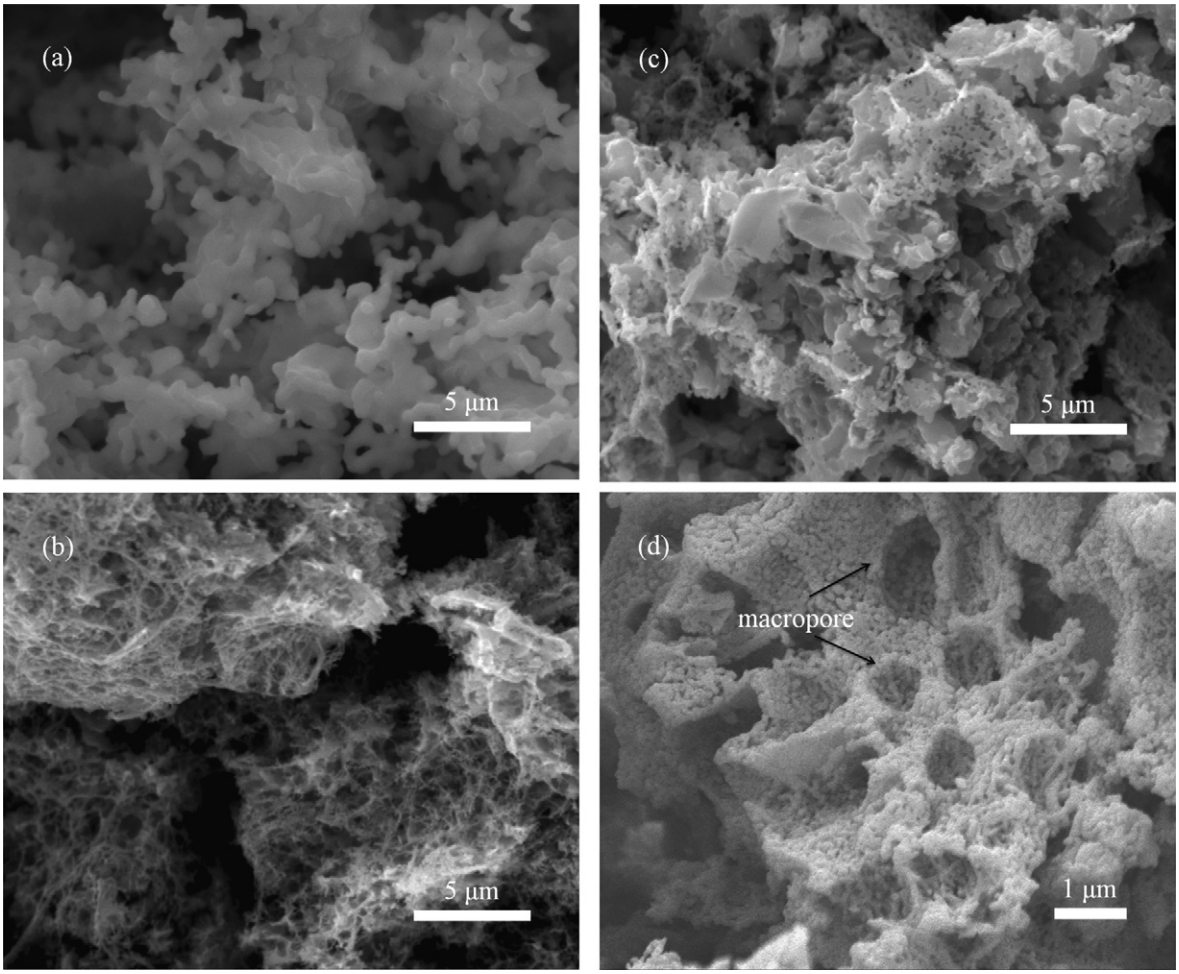

Fig. 2. Cross-sectional views for cathodes: (a) BZCY electrolyte backbone; (b) infiltrated SSC–BZCY cathode; (c) screen-printed SSC–BZCY cathode; and (d) fresh infiltrated SSC–BZCY cathode at high magnification.

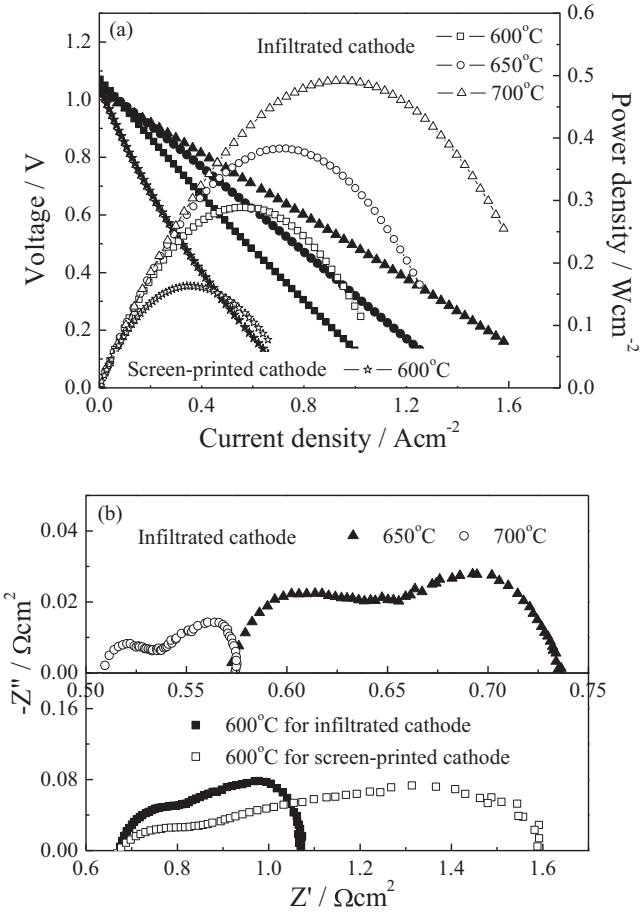

Fig. 3. (a) Cell voltage (solid symbols) and power density (open symbols) as a function of current density for single cells; and (b) impedance spectra of the cells measured under open-circuit conditions.

0.383 and 0.491 W cm^{-2} were achieved at 600, 650 and 700 °C, respectively, showing a comparable cell performance for similar infiltrated cathode reported previously [27]. Shown in Fig. 3(b) are AC impedance spectra of the cell under open-circuit conditions. Total cell resistance (R_t), cell ohmic resistance (R_o), and cell polarization resistance (R_p) were determined from the impedance spectra at different temperatures. As shown in Fig. 3(b), the cell polarization resistances were 0.388, 0.162, and 0.064 Ω cm^2 at 600, 650 and 700 °C, respectively, which were very low for proton-conducting cells. Cell polarization resistances for different cells with the anode material and similar cathode firing temperature were plotted in Fig. 4 [34,35]. At 600 °C, the R_p of infiltrated cathode was much lower than 1.5 Ω cm^2 of a cell based on SSC–BZCY cathode fired at 900 °C, while it was still higher than 0.168 Ω cm^2 for the cell with a cathode firing at 1000 °C [34]. The reason for such differences in the measured cell polarization resistances was probably due to the interparticle connectivity. The adhesion of the cathode to the electrolyte was found to be improved by increasing the firing temperature from 900 to 1000 °C. Though the presence of some second phases such as $BaCoO_3$ and $Sm_2Zr_2O_7$ was observed between BZCY and SSC fired at 1000 °C, the cell performance could still be enhanced due to the reduced contact resistance. Consequently, higher cell performance might be achievable by increasing the firing temperature of infiltrated SSC precursor to improve the connectivity between SSC and BZCY backbone. As shown in Section 2, since the cathode catalyst was coated on the backbone through thermal decomposition process, it was fairly easy to adjust the firing temperature to improve the connectivity between SSC and BZCY

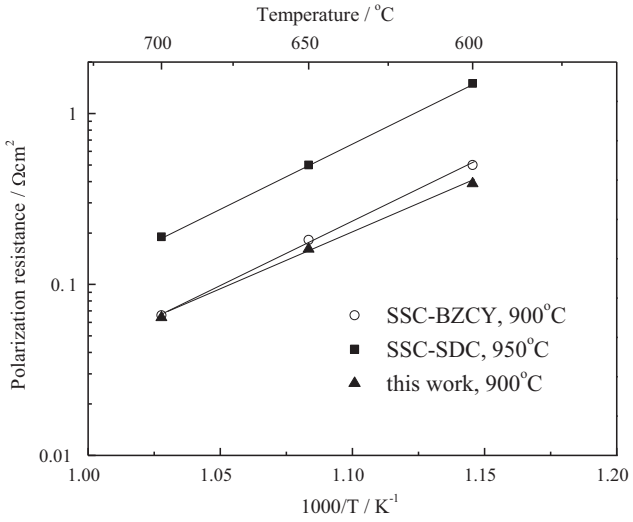

Fig. 4. Polarization resistances determined from impedance spectra for cells: Ni–BZCY|BZCY|SSC–BZCY [34], Ni–BZCY|BZCY|SSC–SDC [35] and Ni–BZCY|BCI|infiltrated SSC–BZCY (this work).

backbone. The effect of firing temperature of the infiltrated precursor on the cathode performance will be systematically evaluated in the future study. At 700 °C, the R_p was comparable to that of the SSC–SDC composite cathode with a cell polarization resistance of 0.066 Ω cm^2 [35]. The apparent activation energy of the infiltrated SSC–BZCY was determined to be 1.32 eV, which was lower than that of 1.48 eV for SSC–SDC cathode, resulting in lower cell polarization resistance. Total cell resistances were 1.064, 0.734, and

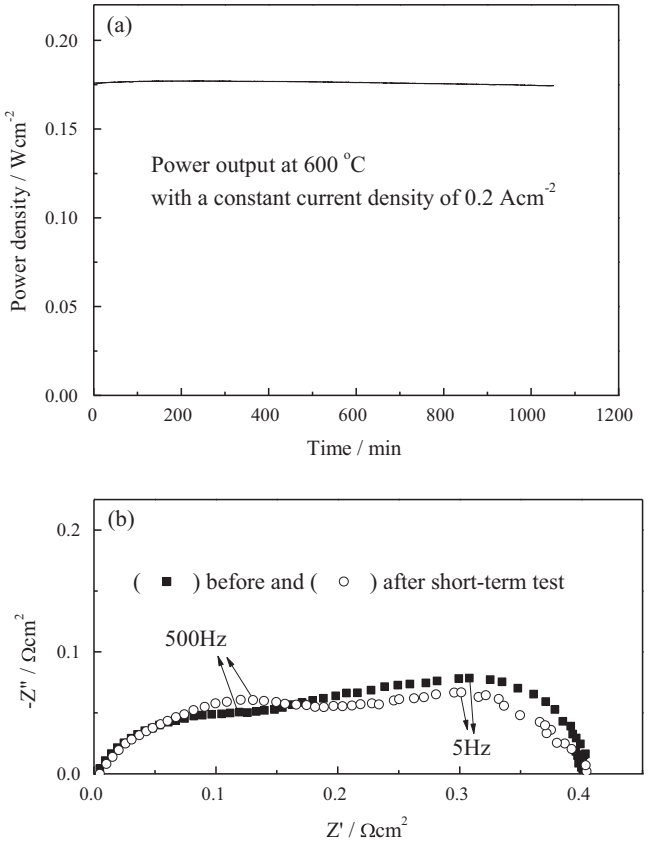

Fig. 5. (a) Short-term durability of cell based on infiltrated SSC–BZCY cathode; and (b) impedance spectra of the cell before and after the short-term test.

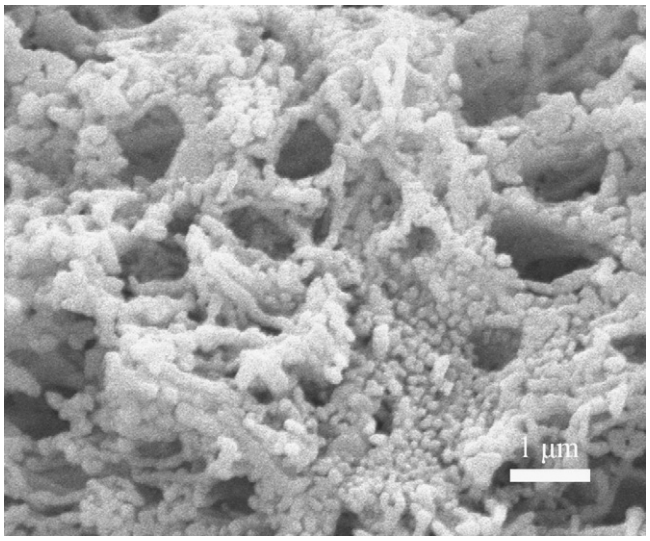

Fig. 6. Cross-sectional view for short-term durability tested infiltrated SSC–BZCY cathode at high magnification.

0.574 Ω cm^2 at 600, 650 and 700 °C, respectively. The ratio of R_p to R_t decreased with the increase in the operating temperatures, from 36.5% at 600 °C to 11.1% at 700 °C, implying that the cell performance was limited not by the polarization resistance but by the ohmic resistance. Consequently, enhanced cell performance may be expected by using thinner electrolyte film or more conducting electrolyte material with good chemical stability such as BZCY or $BaZr_{0.1}Ce_{0.7}Y_{0.1}Yb_{0.1}O_{3-\delta}$ [31,36].

Compared with the infiltrated SSC–BZCY cathode, screen-printed cathode had lower cell performance as shown in Fig. 3(a) and (b). At 600 °C, the cell with screen-printed SSC–BZCY cathode showed a maximum power output of 0.163 W cm^{-2} and a relatively high R_p value of 0.912 Ω cm^2, which was more than 2 times larger than that of the cell based on infiltrated SSC–BZCY cathode. Since the electrolyte and the anode were the same materials with similar thickness and microstructure, lower cell R_p observed in cells with the infiltrated cathode might be attributed to the higher cathode performance due to the unique multiscale porous microstructure providing enhanced mass transport and electrochemical reactions.

The short-term durability of the cell based on the infiltrated SSC–BZCY cathode was also investigated and shown in Fig. 5(a) where the power density was monitored as a function of time with a constant current density of 0.2 A cm^{-2} at 600 °C. The cell power output was fairly stable during the short-term durability test. No obvious increase in cell polarization resistance was observed as shown in Fig. 5(b). Further, there was no significant change in the multiscale porous microstructure of the infiltrated cathode between the tested cell (Fig. 6) and the fresh one (Fig. 2(d)).

4. Conclusions

Multiscale porous SSC–BZCY composite cathode for proton-conducting intermediate temperature SOFCs was successfully fabricated by the infiltration approach. The composite cathode was consisted of BZCY backbones and SSC catalysts with multiscale pores. Single cell based on infiltrated SSC cathode with multiscale porous microstructure demonstrated peak power densities of 0.289, 0.383, and 0.491 W cm^{-2} at 600, 650 and 700 °C, respectively, which were higher than those of cells based on screen-printed SSC–BZCY composite cathode. The multiscale porous SSC–BZCY composite cathode showed remarkably low interfacial polarization resistances of 0.388, 0.162, and 0.064 Ω cm^2 at 600, 650 and 700 °C, respectively. No increase in cell polarization resistance was found for single cell based on infiltrated SSC cathode with multiscale porous microstructure during a short-term durability test.

Acknowledgements

Financial support from NSF (Award no. 1000068), HeteroFoam Center, an EFRC funded by DoE Office of Basic Energy Sciences (Award no. DE-SC0001061) and DoE-NEUP (Award no. 09-510) is gratefully acknowledged.

References

[1] S. Adler, Chem. Rev. 104 (2004) 4791.
[2] H. Iwahara, Solid State Ionics 86–88 (1996) 9.
[3] K. Kreuer, Chem. Mater. 8 (1996) 610.
[4] T. Norby, Solid State Ionics 125 (1999) 1.
[5] K. Kreuer, Annu. Rev. Mater. Res. 33 (2003) 333.
[6] S. Skinner, Int. J. Inorg. Mater. 3 (2001) 113.
[7] S. Souza, S. Visco, L. Jonghe, J. Electrochem. Soc. 144 (3) (1997) L35.
[8] J. Will, A. Mitterdorfer, C. Kleinlogel, D. Perednis, L. Gauckler, Solid State Ionics 131 (2000) 79.
[9] N. Ito, M. Iijima, K. Kimura, S. Iguchi, J. Power Sources 152 (2005) 200.
[10] J. Ding, J. Liu, Solid State Ionics 179 (2008) 1246.
[11] C. Sun, R. Hui, J. Roller, J. Solid State Electrochem. 14 (2010) 1125.
[12] N. Hart, N. Brandon, M. Day, J. Shemilt, J. Mater. Sci. 36 (2001) 1077.
[13] M. Bellino, J. Sacanell, D. Lamas, A. Leyva, N. Reca, J. Am. Chem. Soc. 129 (2007) 3066.
[14] F. Zhao, Z. Wang, M. Liu, L. Zhang, C. Xia, F. Chen, J. Power Sources 185 (2008) 13.
[15] E. Geraud, H. Möhwald, D. Shchukin, Chem. Mater. 20 (2008) 5139.
[16] H. Fukunaga, M. Ihara, K. Sakaki, K. Yamada, Solid State Ionics 86–88 (1996) 1179.
[17] Y. Zhang, S. Zha, M. Liu, Adv. Mater. 17 (2005) 487.
[18] Q. Liu, F. Chen, Mater. Res. Bull. 44 (2009) 2056.
[19] Q. Liu, F. Zhao, X. Dong, C. Yang, F. Chen, J. Phys. Chem. C 113 (2009) 17262.
[20] M. McCamish, J. Chem. Educ. 64 (1987) 710.
[21] G. Whitesides, J. Mathias, C. Seto, Science 254 (1991) 1312.
[22] S. Leininger, B. Olenyuk, P. Stang, Chem. Rev. 100 (2000) 853.
[23] J. Piao, K. Sun, N. Zhang, S. Xu, J. Power Sources 175 (2008) 288.
[24] S. Jiang, Mater. Sci. Eng. A 418 (2006) 199.
[25] T. Sholklapper, H. Kurokawa, C. Jacobson, S. Visco, L. Jonghe, Nano Lett. 7 (2007) 2136.
[26] Z. Jiang, C. Xia, F. Chen, Electrochim. Acta 55 (2010) 3595.
[27] T. Wu, Y. Zhao, R. Peng, C. Xia, Electrochim. Acta 54 (2009) 4888.
[28] F. Zhao, R. Ran, C. Xia, Mater. Res. Bull. 43 (2008) 370.
[29] F. Zhao, S. Wang, K. Brinkman, F. Chen, J. Power Sources 195 (2010) 5468.
[30] F. Zhao, Q. Liu, S. Wang, K. Brinkman, F. Chen, Int. J. Hydrogen Energy 35 (2010) 4258.
[31] C. Zuo, S. Zha, M. Liu, Adv. Mater. 18 (2006) 3318.
[32] L. Bi, S. Zhang, L. Zhang, Z. Tao, H. Wang, W. Liu, Int. J. Hydrogen Energy 34 (2009) 2421.
[33] J. Lü, L. Wang, L. Fan, Y. Li, L. Dai, H. Guo, J. Rare Earth 26 (2008) 505.
[34] L. Yang, C. Zuo, S. Wang, Z. Cheng, M. Liu, Adv. Mater. 20 (17) (2008) 3280.
[35] W. Sun, L. Yan, B. Lin, S. Zhang, W. Liu, J. Power Sources 195 (10) (2010) 3155.
[36] L. Yang, S. Wang, K. Blinn, M.F. Liu, Z. Liu, Z. Cheng, M.L. Liu, Science 326 (2009) 126.